SCIENTIFIC REPORTS

OPEN

SUBJECT AREAS:
ELECTRONIC PROPERTIES AND MATERIALS
MATERIALS FOR ENERGY AND CATALYSIS

Received
15 July 2014

Accepted
8 December 2014

Published
19 January 2015

Correspondence and requests for materials should be addressed to J.H. (hu.junqing@dhu.edu.cn) or W.Z. (apwjzh@cityu.edu.hk)

* These authors contributed equally to this work.

Dendritic Heterojunction Nanowire Arrays for High-Performance Supercapacitors

Rujia Zou[1,2]*, Zhenyu Zhang[1]*, Muk Fung Yuen[1], Junqing Hu[2], Chun-Sing Lee[1] & Wenjun Zhang[1]

[1]Center of Super-Diamond and Advanced Films (COSDAF), Department of Physics and Materials Science, City University of Hong Kong, Hong Kong, [2]State Key Laboratory for Modification of Chemical Fibers and Polymer Materials, College of Materials Science and Engineering, Donghua University, Shanghai 201620, China.

Herein, we designed and synthesized for the first time a series of 3D dendritic heterojunction arrays on Ni foam substrates, with $NiCo_2S_4$ nanowires as cores and $NiCo_2O_4$, NiO, Co_3O_4, and MnO_2 nanowires as branches, and studied systematically their electrochemical performance in comparison with their counterparts in core/shell structure. Attributed to the following reasons: (1) both core and branch are pseudocapacitively active materials, (2) the special dendritic structure with considerable inter-nanowire space enables easy access of electrolyte to the core and branch surfaces, and (3) the highly conductive $NiCo_2S_4$ nanowire cores provide "superhighways" for charge transition, $NiCo_2S_4$-cored dendritic heterojunction electrodes synergistically lead to ultrahigh specific capacitance, good rate capability, and excellent cycling life. These results of core/branch dentritic heterojunction arrays is universially superior to their core/shell conterparts, thus this is a significant improvement of overall electrochemical performance.

The development of new energy storage techniques is a vital link in the applications of renewable energy sources[1,2]. Among the current protocols, supercapacitor is considered as one of the most ideal candidates for energy storage due to its fast charging and discharging capability, high power density, long lifespan and operation safety[3,4]. Based on their charge-storage mechanism, supercapacitors are generally classified into two categories: electrical double-layer capacitors (EDLCs) that use carbon-active materials and pseudocapacitors that use redox-active materials[1,2]. In recent years extensive research has been focused on pseudocapacitors because their energy density associated with Faradaic reactions is substantially larger by at least one order of magnitude than that of EDLCs[3]. The characters of electrode materials have been known to be predominant in determining the performance of a pseudocapacitor. Among the electrode materials studied thus far, transition metal oxides (MnO_2, NiO, V_2O_5, Co_3O_4, $NiCo_2O_4$ etc.) and sulfides (CoS_2, NiS_2, WS_2 etc.) have shown great potentials. These materials are low cost, environmentally benign and naturally abundant; moreover, they can be synthesized by facile, cost-effective and scalable techniques, such as hydro/solvothermal growth method and electrodeposition[1,4–6]. However, these oxides and sulfides have in general a poor electric conductivity, and the electrodes made of a single component of these materials could not satisfy the requirement of fast electron transport in a high-performance supercapacitor[1,7].

A feasible approach to apply these active electrode materials in pseudocapacitors is to composite them with carbon nanomaterials[8–11] and inorganic[12–15] conductive components in core-shell configuration and to prepare them in three-dimensional (3D) nanostructure arrays. The 3D topography has a large surface area and short diffusion paths for both electron and ions. Moreover, these 3D composite materials could be applied directly as electrodes in pseudocapacitors, avoiding the "dead volume" of polymer binder used in conventional film electrode preparation[7,16]. In the core-shell composites reported thus far, a group of studies employed conductive oxide nanostructures such as TiO_2, WO_{3-x}, SnO_2 and ZnO nanorod arrays as the core materials, in which the cores could provide effective electron transport path but they could not contribute to capacitance[17–20]. Another group was based on with redox-active nanowire cores, e.g., Co_3O_4@MnO_2, Ni_3S_2@$Ni(OH)_2$, $NiCo_2O_4$@MnO_2, $NiCo_2O_4$@NiO core-shell heterostructures (CSHs)[12–15]. In these designs, however, the core materials had limited contribution to capacitance because they were almost completely blocked from the access of electrolyte by the shells. In addition, the poor electric conductivity of the core materials also deteriorated the cycling rate of the capacitors[21–23]. Therefore, to develop a new heterostructure, within which the core material has the merits of high

specific capacitance, good electric conductivity, and high ion accessibility, would benefit the further improvement of the overall performance of pseudocapacitors.

In the present work, we designed and synthesized on Ni foam substrates a series of 3D dendritic heterojunction (DH) arrays with $NiCo_2S_4$ nanowires as cores and $NiCo_2O_4$, NiO, Co_3O_4, and MnO_2 nanowires as branches, and evaluated their electrochemical performance. $NiCo_2S_4$ has a high electric conductivity (~100 times of that of $NiCo_2O_4$, and about four orders of magnitude higher than those of the conventional metal oxide semiconductors)[6]. More significantly, $NiCo_2S_4$ has also a comparable specific capacitance to that of $NiCo_2O_4$[6,24]. Compared with the corresponding 3D CSHs, the 3D DH arrays were shown to have drastically improved pseudocapacitive performances, which was assigned to the synergistic effects of both special morphology design and the rational selection of component materials in the heterostructures. In the 3D DH arrays, the $NiCo_2S_4$ nanowire cores not only serve as highly conductive electron transport path but also an active element to contribute to capacitance, and the branched metal oxide nanowires provide enhanced redox reaction sites and as well enable the permeation of electrolyte to the cores.

Results

$NiCo_2S_4$ nanowires arrays were synthesized by sulfurization of NiCo-precursor nanowire arrays grown by hydrothermal method on Ni foam substrates (Figure S1)[25,26]. The scanning electron microscopy (SEM) image in Figure 1a shows that a large scale $NiCo_2S_4$ nanowires with a length of ~ 5 μm were uniformly grown on the Ni foam. Close observation revealed that the nanowires had a gradually shrunk diameter from ~150 nm at bottom to ~20 nm at top, and the nanowires were in a hollow structure (Figure S2a). The $NiCo_2S_4$ nanowires preserved the morphology of NiCo-precursor nanowires, and the formation of hollowed structure was due to etching of the interior components by the acidic solution during the sulfurization process[26]. Moreover, the hollowed $NiCo_2S_4$ nanowires had a single crystalline structure, as evidenced by the high-resolution transmission electron microscopy (HRTEM) image in Figure S2b. The XRD pattern in Figure S3 also verified the growth of crystalline $NiCo_2S_4$ in cubic phase.

The electrically conductive $NiCo_2S_4$ nanowires were employed as the trunks or cores for the further growth of heterogeneous branched electroactive materials by hydrothermal method. Figure 1b presents an SEM image of the $NiCo_2S_4/NiCo_2O_4$ DH arrays after subjected to a post annealing process. Enlarged SEM image in Figures 1c and TEM image in Figure 1d reveal that the $NiCo_2O_4$ branched nanowires were distributed evenly along the $NiCo_2S_4$ nanowire length, forming $NiCo_2S_4/NiCo_2O_4$ DH arrays. The $NiCo_2O_4$ branched nanowires have a diameter of 20–30 nm and the length of $NiCo_2O_4$ nanowires ranges from 2 to 3 μm. The $NiCo_2S_4/NiCo_2O_4$ DH is featured with open space between branched nanowires, which allows access of electrolyte to both branch and core surfaces and leads to improved electrochemical performance as discussed below. The $NiCo_2O_4$ branched nanowires have a mesoporous structure with the pore size ranging from 2 to 5 nm (Figure S4a), which has been demonstrated to be due to the release of H_2O and gases during the intermediates' decomposition/oxidation by annealing[27]; and the HRTEM image in Figure S4b confirmed the crystal nature of $NiCo_2O_4$ branches. The mesoporous structure of $NiCo_2O_4$ nanowires may increase the electrode/electrolyte contact area and thus the active sites for electrochemical reaction[1]. Moreover, the direct growth of $NiCo_2O_4$ branched nanowires from $NiCo_2S_4$ core nanowires (as revealed by the HRTEM image in the inset of Figure 1d, the heterojunction area is denoted by the blue arrow) may facilitate the electron transport from $NiCo_2S_4$ core to $NiCo_2O_4$ branch nanowires.

Figure 1e shows XRD pattern of the as-synthesized $NiCo_2S_4/NiCo_2O_4$ DH arrays scratched from Ni substrates and the standard diffractions of $NiCo_2O_4$ (Joint Committee on Powder Diffraction Standards (JCPDS) card No. 20-0781) and $NiCo_2S_4$. (JCPDS No. 20-0782). The result further verifies that $NiCo_2S_4/NiCo_2O_4$ DHs were achieved. As a reference sample, $NiCo_2S_4$@$NiCo_2O_4$ CSH array was also synthesized on Ni foam substrate, as shown in Figure 1f. Dense $NiCo_2O_4$ nanosheets were packed around the $NiCo_2S_4$ nanowire cores. Comprehensive structure characterization in Supporting Information I and Figure S5 elucidate that the $NiCo_2S_4$ nanowire

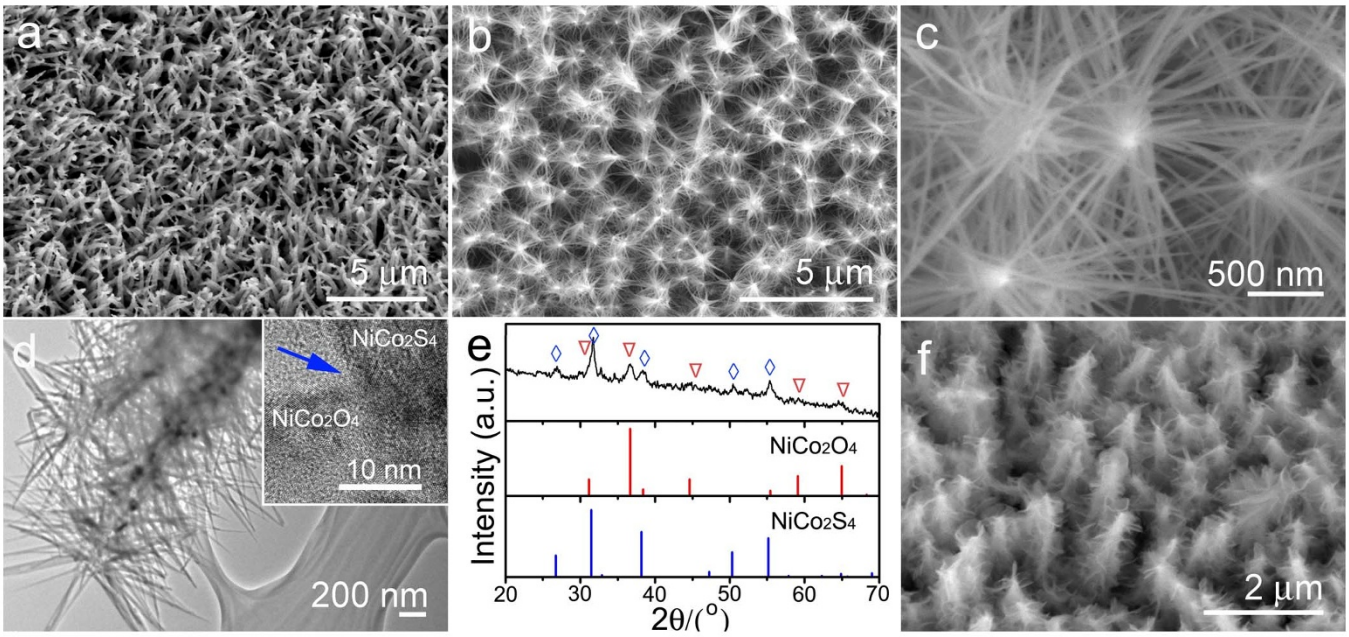

Figure 1 | (a) SEM morphology of the as-synthesized hollow $NiCo_2S_4$ nanowire arrays on Ni foam. (b) and (c) SEM images of $NiCo_2S_4/NiCo_2O_4$ DH arrays on Ni foam with different magnification. (d) TEM image of $NiCo_2S_4/NiCo_2O_4$ DHs. The inset shows the HRTEM image of joint region between $NiCo_2S_4$ core and a $NiCo_2O_4$ branch nanowire. (e) XRD pattern of the $NiCo_2S_4/NiCo_2O_4$ DH arrays scratched from Ni foam. (f) SEM image of the reference $NiCo_2S_4$@$NiCo_2O_4$ CSH arrays synthesized on Ni foam.

surfaces were entirely covered with interconnected $NiCo_2O_4$ nanosheets, forming a typical core-shell heterostructure.

The electrochemical properties of $NiCo_2S_4/NiCo_2O_4$ DH arrays on Ni foam were comparatively studies, with the control experiments on reference samples of $NiCo_2S_4@NiCo_2O_4$ CSH arrays and $NiCo_2S_4$ nanowire arrays, in a standard three-electrode configuration using 1.0 M KOH electrolyte. Figure 2a shows the cyclic voltammetry (CV) curves of $NiCo_2S_4/NiCo_2O_4$ DH arrays at different scan rates of 5, 10, and 20 mV s^{-1} in a potential window of -0.3 to 0.6 V. The CV curves with clear redox peaks mainly caused by Faradaic redox reactions indicate the pseudocapacitive characteristics of the $NiCo_2S_4/NiCo_2O_4$ DH[28]. With the increase in scan rate from 2 to 20 mV s^{-1}, the anodic peaks shift toward high potential and the cathodic peaks move toward negative potential simultaneously, which could be attributed to the polarization caused by high scan rate. The CV curves maintain an unchanged shape even at a high scan rate, implying that the electrode enables excellent electrochemical reversibility and high-rate performance. For the $NiCo_2S_4/NiCo_2O_4$ DH sample, an almost linear relationship has been observed between anodic peak current density and the applied scan rate, as shown in Figure S6, which indicates the occurrence of surface redox reactions during the charge storage process[29]. The CV of $NiCo_2S_4@NiCo_2O_4$ CSH arrays at a scan rate of 10 mV s^{-1} was also plotted in Figure 2a (pink dotted line), which presents the similar shape as those of $NiCo_2S_4/NiCo_2O_4$ DH. However, at the same scan rate, the $NiCo_2S_4/NiCo_2O_4$ DH electrode has an obviously larger CV integrated area than that of $NiCo_2S_4@NiCo_2O_4$ CSH electrode, suggesting that the $NiCo_2S_4/NiCo_2O_4$ DH electrode has a much increased capacitance as compared with $NiCo_2S_4@NiCo_2O_4$ CSH electrode.

The galvanostatic charge-discharge (CD) tests of $NiCo_2S_4/NiCo_2O_4$ DH arrays were conducted in a potential window between 0 and 0.45 V at discharge current densities ranging from 5 to 50 mA cm^{-2}, as shown in Figure 2b. According to the areal capacitances formula[1,7,8], the discharge areal capacitance is calculated to be 7.13, 5.82, 4.57, 3.93, 3.38, 3.17 F cm^{-2} at current densities of 5, 10, 20, 30, 40, and 50 mA cm^{-2}, respectively, as shown in Figure 2c (black curve). Similarly, the areal capacitance of $NiCo_2S_4@NiCo_2O_4$ CSH electrode (Figure 2c, red curve) and $NiCo_2S_4$ nanowire electrode was also evaluated, as depicted by the red and blue curves in Figure 2c, respectively. It is revealed that a higher areal capacitance is achieved with the DH electrode at the current density of 10 mA cm^{-2} (5.82 F cm^{-2} for $NiCo_2S_4/NiCo_2O_4$ DH versus 2.81 F cm^{-2} for $NiCo_2S_4@NiCo_2O_4$ CSH and 1.02 F cm^{-2} for $NiCo_2S_4$ nanowire electrodes). Impressively, at an elevated current density of 50 mA cm^{-2}, the improvement is more significant (3.17 F cm^{-2} for $NiCo_2S_4/NiCo_2O_4$ DH, ~4 times larger than that of $NiCo_2S_4@NiCo_2O_4$ CSH (0.88 F cm^{-2}) and ~10 times larger than that of $NiCo_2S_4$ nanowire electrodes (0.312 F cm^{-2}). For the current density increase from 10 to 50 mA cm^{-2}, the rate capability of $NiCo_2S_4/NiCo_2O_4$ DH, $NiCo_2S_4@NiCo_2O_4$ CSH and $NiCo_2S_4$ nanowire electrodes are 54.5%, 31.3% and 30.6%, respectively.

The cycling stability of $NiCo_2S_4/NiCo_2O_4$ DH electrode was evaluated by repeated charge-discharge measurements at a scan rate of 50 mVs^{-1}, as shown in Figure 2d (black curve). The overall capacitance loss after 3000 cycles was less than 4.8%, i.e., the capacitance retention for 3000 cycles was 95.2%, which is comparable to that of single-component $NiCo_2S_4$ nanowire array electrode (95.8%), but superior to that of $NiCo_2S_4@NiCo_2O_4$ CSH electrode (88.8%).

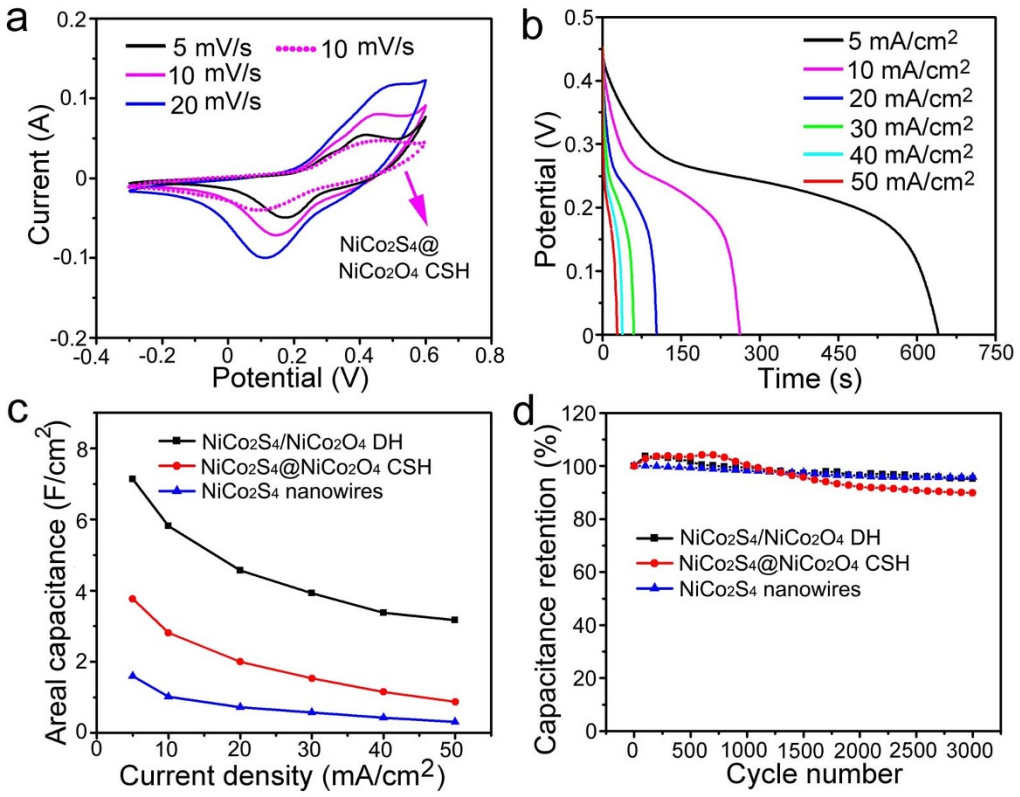

Figure 2 | Electrochemical properties of $NiCo_2S_4/NiCo_2O_4$ DH, $NiCo_2S_4@NiCo_2O_4$ CSH and $NiCo_2S_4$ nanowire electrodes in 1 M KOH aqueous solution at room temperature. (a) CV curves at different scan rates recorded from electrodes consisting of $NiCo_2S_4/NiCo_2O_4$ DH electrode. The CV curve of $NiCo_2S_4@NiCo_2O_4$ CSH electrode measured at a scan reate of 10 mV/s is also shown by the pink dotted line as a reference. (b) Discharge curves of $NiCo_2S_4/NiCo_2O_4$ DH electrode at different current densities. (c) Areal capacitance of $NiCo_2S_4/NiCo_2O_4$ DH, $NiCo_2S_4@NiCo_2O_4$ CSH, and $NiCo_2S_4$ nanowire electrodes at different current densities. (d) Cycling properties of $NiCo_2S_4/NiCo_2O_4$ DH, $NiCo_2S_4@NiCo_2O_4$ CSH, and $NiCo_2S_4$ nanowire electrodes in 3000 cycles at 50 mVs^{-1}.

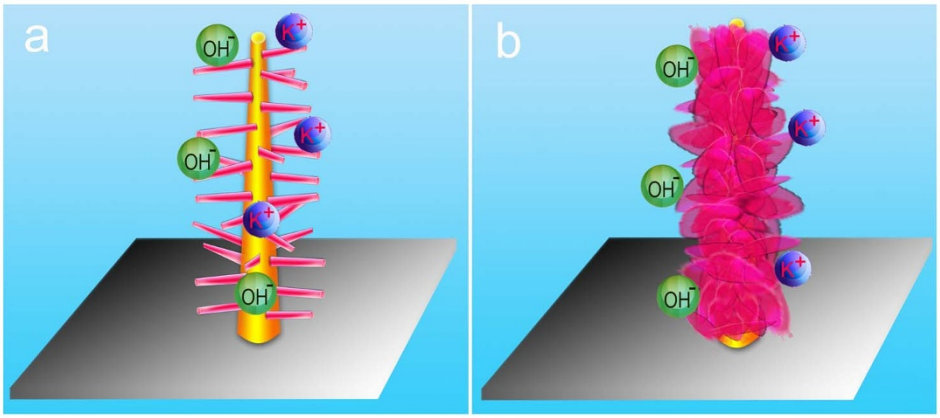

Figure 3 | Schematic illustration showing the structural characteristics of (a) DH and (b) CSH electrodes.

Moreover, it is also noted that the capacitance of $NiCo_2S_4$@$NiCo_2O_4$ CSH electrode increases gradually in about the first several hundred cycles and then starts to decrease, which is considered to be due to slow activation of active electrode material as in previous reports[30,31]. In contrast, the $NiCo_2S_4$/$NiCo_2O_4$ DH electrode reaches its capacitance maximum quickly in about the first several cycles, indicating that the dendritic structure is much easier to be activated. The dendritic nanostructure may lead to facile exposure of whole surface of each of its component to the electrolyte for activation, and the joule heat generated in redox reactions can also be effectively dissipated to electrolyte[22–34]. Therefore, the DH electrode has an improved stability as compared to CSH electrode, suggesting another advantage of the DH electrode in energy storage.

The structural stability of the $NiCo_2S_4$@$NiCo_2O_4$ DH, $NiCo_2S_4$@$NiCo_2O_4$ CSH and $NiCo_2S_4$ nanowires after 3000 cycles at the scan rate of 50 mV/s is confirmed as shown in Figure S7. Firstly, as shown in Figure S7a, the electrode of $NiCo_2S_4$@$NiCo_2O_4$ DH could still retain its integrity well, except for the increased roughness on the electrode surface and some expansion, and fracture of branch nanowires caused by the redox reactions during the repeated charge/discharge processes, suggesting the stable structure of the DH architecture. Secondly, the electrode of $NiCo_2S_4$@$NiCo_2O_4$ CSH can not retain its integrity structures well, as shown in Figure S7b. The electrode surface becoming more rough and the structure of $NiCo_2S_4$@$NiCo_2O_4$ CSH have merged, expanded and fractured, which were also caused by the redox reactions during the repeated charge/discharge processes. Especially, $NiCo_2S_4$ nanowires were more closely covered by $NiCo_2O_4$ shell than that of originally shell structure after cycles. So, the active sites of $NiCo_2S_4$ core nanomaterials were largely invalidated by covered $NiCo_2O_4$ shell nanomaterials, and some active sites of shell materials would also be hindered by covered shell materials in 3D CSH electrode systems, which significantly weaken the synergistic effect between different components and further decreased supercapacitor performances. Finally, the electrode of $NiCo_2S_4$ nanowire arrays still retain its integrity well (Figure S7c), except for the slightly increased roughness on the electrode surface caused by volume change during the the redox reactions. The structure stability of the $NiCo_2S_4$ nanowire arrays resulted in the good cycling performance.

Discussion

The $NiCo_2S_4$/$NiCo_2O_4$ DH electrode shows obviously higher areal capacitance over that of $NiCo_2S_4$@$NiCo_2O_4$ CSH electrode, although the $NiCo_2S_4$@$NiCo_2O_4$ CSH electrode has already far greater areal capacitance than those of previously reported pure $NiCo_2O_4$ nanostructures[35,36] and composite electrodes in core/shell heterostructure, such as MnO_2@$NiCo_2O_4$ (2.01 F cm^{-2} at 2 mA cm^{-2})[14], MnO_2@Co_3O_4 (0.56 F cm^{-2} at 11.25 cm^{-2})[21], NiO@Co_3O_4 (1.35 F cm^{-2} at 6 mA cm^{-2})[37], NiO@MnO_2 (0.35 F cm^{-2} at 9.5 mA cm^{-2})[23], and NiO@TiO_2 (3 F cm^{-2} at 0.4 mA cm^{-2})[38], $NiCo_2O_4$@$NiCo_2O_4$ (1.55 F cm^{-2} at 2 mA cm^{-2})[39], and $Co_xNi_{1-x}(OH)_2$@$NiCo_2S_4$ (2.86 F cm^{-2} at 4 mA cm^{-2})[24]. The outstanding capacitive properties of $NiCo_2S_4$/$NiCo_2O_4$ DH electrode are considered to originate from the synergistic effect of its following distinctive compositional and topological features. First, both core and branch are pseudocapacitively active materials; and the 3D dendritic structure with considerable inter-nanowire space enables easy access of electrolyte to the core and branch surfaces, as illustrated in Figure 3a and Figure S8a. Therefore, both of them can effectively contribute to the capacitance. In contrast, in the $NiCo_2S_4$@$NiCo_2O_4$ CSH (as depicted in Figure 3b and Figure S8b), the $NiCo_2S_4$ core nanowire is entirely covered with $NiCo_2O_4$ nanosheets, and the $NiCo_2S_4$ core nanowire can hardly provide active sites for redox reactions. Secondly, the $NiCo_2S_4$ nanowire cores directly grown on Ni foam are highly conductive, which act as not only a robust host for branched nanowires but also provide "superhighways" for charge in the DH structure. The direct growth of branched $NiCo_2O_4$ nanowires on $NiCo_2S_4$ core nanowires further guarantee the effective charge transport between them. Moreover, the $NiCo_2S_4$/$NiCo_2O_4$ DH electrode also has the following characteritics which have been demonstrated to be beneficial to capacitance improvement[12–15]. the mesoporous nature of $NiCo_2O_4$ branched nanowires that increases the electroactive sites and the direct growth of electrode on conductive substrate that avoids the use of polymer binder/conductive additives.

In order to further verify the superiority of DH design for electrode application in supercapacitors, we synthesized a series of 3D DH arrays with various of branched nanowires grown on $NiCo_2S_4$ core nanowires, including $NiCo_2S_4$/NiO DH (Figure 4a), $NiCo_2S_4$/Co_3O_4 DH (Figure 4b), and $NiCo_2S_4$/MnO_2 DH (Figure 4c) arrays on Ni foam substrates. The corresponding CSHs arrays were also synthesized on Ni foam substrate, as shown in Figures 4g–i. It can be seen that NiO, Co_3O_4, and MnO_2 branched nanowires were uniformly grown on $NiCo_2S_4$ core nanowires. The diameters of branched nanowires are: ~30 nm for NiO, ~20 nm for Co_3O_4, and ~10 nm for MnO_2; and their lengths are: 1 to 2 μm for NiO, 2-3 μm for Co_3O_4, and ~100 nm for MnO_2. It was also confirmed by TEM observations that NiO and Co_3O_4 nanowires are mesoporous with pore size ranging from 2 to 5 nm, and MnO_2 nanowires do not have the mesoporous structure (Figure S9). For the corresponding CSH samples, like $NiCo_2S_4$@$NiCo_2O_4$ CSH arrays, the $NiCo_2S_4$ nanowire surfaces were entirely covered with interconnected and dense NiO, Co_3O_4, and MnO_2 nanosheets. More detailed TEM and XRD characterization of the DH and CSH arrays can be found in Supporting Information II and III and Figure S10.

The electrochemical performance of $NiCo_2S_4$/NiO, $NiCo_2S_4$/Co_3O_4, $NiCo_2S_4$/MnO_2 DH electrodes and the their CSH counter-

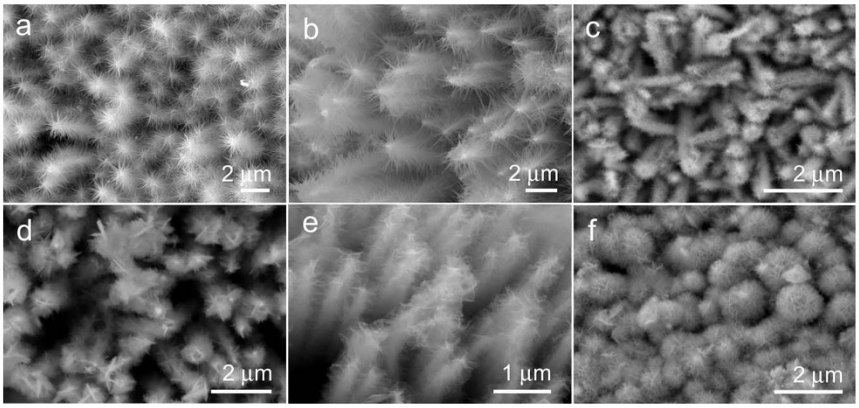

Figure 4 | **SEM images of (a) $NiCo_2S_4$/NiO DH, (b) $NiCo_2S_4$/Co_3O_4 DH, (c) $NiCo_2S_4$/MnO_2 DH, (d) $NiCo_2S_4$@NiO CSH, (e) $NiCo_2S_4$@Co_3O_4 CSH, (f) $NiCo_2S_4$@MnO_2 CSH arrays on Ni foam substrates.**

parts were tested. Figure S12 gives the CV curves of the $NiCo_2S_4$/MnO_2, $NiCo_2S_4$/NiO, $NiCo_2S_4$/Co_3O_4 DH electrodes in comparison with those of their corresponding CSH electrodes at scan rate of 10 mVs^{-1} and potential window from −0.3 to 0.6 V. Obviously, all CV curves show the pseudocapacitive characteristics, and the shape of CV curves of corresponding DH and CSH samples are almost identical. The CD measurements are also performed in the voltage range of 0–0.45 V at a current density of 10 mA cm^{-2} (Figure S13a). In contrast to the CSH electrodes, no obvious fast potential drop was observed in the discharge curves of DH electrodes, indicating that the areal capacitance of DH electrode is much higher than that of its corresponding CSH electrode.

Based on CD measurements at different current densities from 10 to 50 mA cm^{-2}, the areal capacitances of the DH and CSH electrodes were derived, as shown in Figure 5a. The $NiCo_2S_4$/MnO_2, $NiCo_2S_4$/NiO, $NiCo_2S_4$/Co_3O_4 DH electrodes delivered areal capacitances of 10.99 F cm^{-2}, 6.83 F cm^{-2}, 7.47 F cm^{-2} at current density of 10 mA cm^{-2}, and still maintained at 7.29 F cm^{-2}, 4.28 F cm^{-2}, 3.99 F cm^{-2} at current density of 50 mA cm^{-2}. As reference, $NiCo_2S_4$@NiO, $NiCo_2S_4$@Co_3O_4, $NiCo_2S_4$@MnO_2 CSH electrodes showed areal capacitances of 6.64 F cm^{-2}, 4.57 F cm^{-2}, 3.31 F cm^{-2}, respectively, at current density of 10 mA cm^{-2}, and 3.26 F cm^{-2}, 0.99 F cm^{-2}, 1.31 F cm^{-2}, respectively, at current density of 50 mA cm^{-2}. For the current density increase from 10 to 50 mA cm^{-2}, the rate capability of $NiCo_2S_4$/MnO_2, $NiCo_2S_4$/NiO, and $NiCo_2S_4$/Co_3O_4 DH electrodes are 66.3%, 62.7%, and 53.6%, respectively, which are much higher than those of corresponding CSH electrodes (49.1%, 21.8%, and 39.7%, respectively). To have a clearer image about the capability of DH electrodes in improving psudocapacitive performance, the areal capacitance of different DH (red column) and CSH (blue column) electrodes at current densities of 10 mA cm^{-2} (dark color) and 50 mA cm^{-2} (light color) is summarily plotted in Figure 5b. It is obvious that all DH electrodes have much increased areal capacitance than their CSH counterpart electrodes. Noticeably, the areal capacitance of DH electrodes at the current density of 50 mA cm^{-2} is comparable or even higher than those of their corresponding CSH electrodes obatained at current density 10 mA cm^{-2}.

Finally, the cycling stabilities of different DH and CSH electrodes were evaluated by repeated charging/discharging measurements at a scan rate of 50 mVs^{-1} for 3000 cycles, as shown in Figure S13b. The overall capacitance retention of $NiCo_2S_4$/NiO, $NiCo_2S_4$/Co_3O_4, $NiCo_2S_4$/MnO_2 DH electrodes after 3000 cycles are ~96.36%, 92.6%, and 92.52%, respectively; and the capacitance retention of $NiCo_2S_4$@NiO, $NiCo_2S_4$@Co_3O_4, $NiCo_2S_4$@MnO_2 CSH electrodes are ~92.71%, 125.84% and 89.39%, respectively. The results suggest that DH electrodes have also better cycling stability than CSH electrodes. The much improved capacitance and better cycling stability clearly clarify the superiority of DH over CSH in the electrode application of psudocapacitors.

In summary, a series of 3D $NiCo_2S_4$-cored DH nanowire arrays, including $NiCo_2S_4$/$NiCo_2O_4$, $NiCo_2S_4$/NiO, $NiCo_2S_4$/Co_3O_4, and $NiCo_2S_4$/MnO_2, were synthesized on Ni foam substrates using a simple hydrothermal reaction combined with a post annealing process. In comparison with their CSH counterpart electrodes, both cores and branches in 3D DH arrays effectively contribute to the capacitance, and the $NiCo_2S_4$ nanowire cores grown directly on Ni

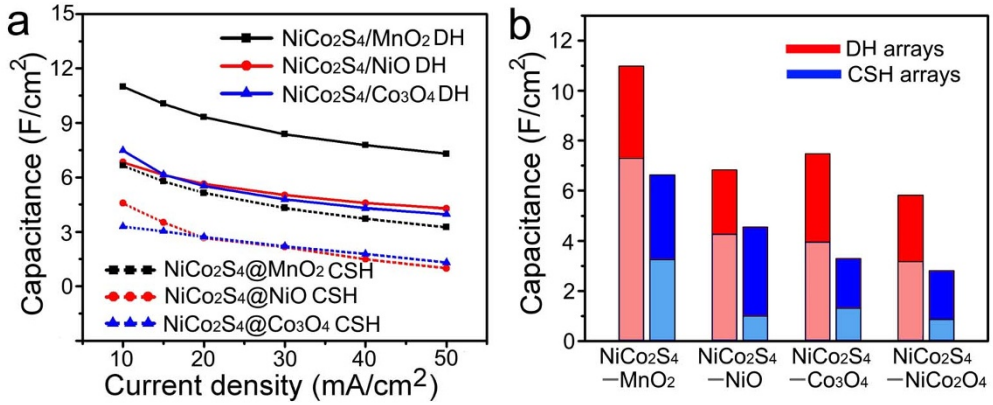

Figure 5 | (a) Areal capacitance of $NiCo_2S_4$/MnO_2, $NiCo_2S_4$/NiO, $NiCo_2S_4$/Co_3O_4 DH elctrodes and $NiCo_2S_4$@MnO_2, $NiCo_2S_4$@NiO, $NiCo_2S_4$@Co_3O_4 CSH electrodes at different current densities. (b) Comparison of areal capacitanc of different DH (red) and CSH (blue) electrodes at current densities of 10 mA cm^{-2} (dark color) and 50 mA cm^{-2} (light color).

foam act as not only a robust host for branched nanowires but also provide "superhighways" for charge in the DH structure. The special geometry and the rational selection of component materials synergistically lead to ultrahigh specific capacitance, good rate capability, and excellent cycling life of DH electrodes. The DH design may provide a universal approach for the development of new electrode materials in high-performance psudocapacitors.

Methods

Synthesis. All commercially available chemicals from Sigma-Aldrich were used as received without further purification. The $NiCo_2S_4$/$NiCo_2O_4$, $NiCo_2S_4$/NiO, $NiCo_2S_4$/Co_3O_4, $NiCo_2S_4$/MnO_2 DH arrays and the corresponding $NiCo_2S_4$@$NiCo_2O_4$, $NiCo_2S_4$@NiO, $NiCo_2S_4$@Co_3O_4, $NiCo_2S_4$@MnO_2 CSH arrays were synthesized on Ni foam using the hydrothermal reactions followed by a post annealing process. The detailed conditions for synthesizing DH and CSH arrays, e.g, source materials, processing temperature, and time, are given Supporting Information IV.

Characterization. The morphology and microstructure of samples were characterized by scanning electron microscopy (SEM, Philips XL 30FEG) and transmission electron microscopy (TEM, Philips FEG TEM CM 200 operated at 200 kV). The X-ray diffraction (XRD) patterns were recorded using a Philips X'Pert MRD X-ray diffractometer with Cu Ka radiation.

Electrochemical measurements. The electrochemical performances of the DH and CSH electrode materials were assessed on an Autolab (PGSTAT302N potentiostat) using a three-electrode mode in 1 M KOH solution. The reference electrode and counter electrode were Ag/AgCl and platinum, respectively. The nominal areas of the DH and CSH electrodes immersed in the electrolyte were controlled to be around 1 cm × 1 cm.

1. Wang, G. P., Zhang, L. & Zhang, J. J. A review of electrode materials for electrochemical supercapacitors. *Chem. Soc. Rev.* **41**, 797 (2012).
2. Jiang, J. *et al*. Recent advances in metal oxide-based electrode architecture design for electrochemical energy storag. *Adv. Mater.* **24**, 5166 (2012).
3. Lang, X. Y., Hirata, A., Fujita, T. & Chen, M. W. Nanoporous metal/oxide hybrid electrodes for electrochemical supercapacitors. *Nat. Nanotechnol.* **6**, 232 (2011).
4. Peng, S. J. *et al.* MS_2 (M = Co and Ni) hollow spheres with tunable interiors for high-performance supercapacitors and photovoltaics. *Adv. Funct. Mater.* **24**, 2155 (2014).
5. Chen, H. C. *et al*. D. D. Highly conductive $NiCo_2S_4$ urchin-like nanostructures for high-rate pseudocapacitors. *Nanoscale* **5**, 8879 (2013).
6. Yu, L., Zhang, L., Wu, H. B. & Lou, X. W. Formation of $Ni_xCo_{3-x}S_4$ hollow nanoprisms with enhanced pseudocapacitive properties. *Angew. Chem. Int. Edit.* **53**, 3711 (2014).
7. Yan, J., Wang, Q., Wei, T. & Fan, Z. J. Recent advances in design and fabrication of electrochemical supercapacitors with high energy densities. *Adv. Energy Mater.* **4**, 1300816 (2014).
8. Cao, X. H., Yin, Z. Y. & Zhang, H. Three-dimensional graphene materials: preparation, structures and application in supercapacitors. *Energy Environ. Sci.* **7**, 1850 (2014).
9. Wang, K., Wu, H. P., Meng, Y. N. & Wei, Z. X. Conducting polymer nanowire arrays for high performance supercapacitors. *Small* **10**, 14 (2014).
10. Zhu, J. X., Yang, D., Yin, Z. Y., Yan, Q. Y. & Zhang, H. Graphene and graphene-based materials for energy storage applications. *Small* **10**, 3480 (2014)
11. Cao, X. H. *et al*. Preparation of novel 3D graphene networks for supercapacitor applications. *Small* **7**, 3163 (2011).
12. Liu, J. P. *et al*. Co_3O_4 nanowire@MnO_2 ultrathin nanosheet core/shell arrays: a new class of high-performance pseudocapacitive materials. *Adv. Mater.* **23**, 2076 (2011).
13. Zhou, W. J. *et al*. One-step synthesis of Ni_3S_2 nanorod@$Ni(OH)_2$ nanosheet core-shell nanostructures on a three-dimensional graphene network for high-performance supercapacitors. *Energy Environ. Sci.* **6**, 2216 (2013).
14. Yu, L., Zhang, G. Q., Yuan, C. Z. & Lou, X. W. Hierarchical $NiCo_2O_4$@MnO_2 core-shell heterostructured nanowire arrays on Ni foam as high-performance supercapacitor electrodes. *Chem. Commun.* **49**, 137 (2013).
15. Yang, W. L. *et al.* Hierarchical $NiCo_2O_4$@NiO core-shell hetero-structured nanowire arrays on carbon cloth for a high-performance flexible all-solid-state electrochemical capacitor. *J. Mater. Chem. A* **2**, 1448 (2014).
16. Beidaghia, M. & Gogotsi, Y. Capacitive energy storage in micro-scale devices: recent advances in design and fabrication of micro-supercapacitors. *Energy Environ. Sci.* **7**, 867 (2014).
17. Lu, X. H. *et al.* H-TiO_2@MnO_2//H-TiO_2@C core-shell nanowires for high performance and flexible asymmetric supercapacitors. *Adv. Mater.* **25**, 267 (2013).
18. Lu, X. H. *et al*. WO_{3-x}@Au@MnO_2 core-shell nanowires on carbon fabric for high-performance flexible supercapacitors. *Adv. Mater.* **24**, 938 (2012).
19. Yan, J., Khoo, E., Sumboja, A. & Lee, P. S. Facile coating of manganese oxide on tin oxide nanowires with high-performance capacitive behavior. *ACS Nano* **4**, 4247 (2010).
20. He, Y. B., Li, G. R., Wang, Z. L., Su, C. Y. & Tong, Y. X. Single-crystal ZnO nanorod/amorphous and nanoporous metal oxide shell composites: controllable electrochemical synthesis and enhanced supercapacitor performances. *Energy Environ. Sci.* **4**, 1288 (2011).
21. Huang, M. *et al.* Merging of Kirkendall growth and Ostwald ripening: CuO@MnO_2 core-shell architectures for asymmetric supercapacitors. *Sci. Rep.* **4**, 4518 (2014).
22. Xia, H. *et al*. Hierarchically structured Co_3O_4@Pt@MnO_2 nanowire arrays for high-performance supercapacitors. *Sci. Rep.* **3**, 2978 (2013).
23. Liu, J. P., Jiang, J., Bosman, M. & Fan, H. J. Three-dimensional tubular arrays of MnO_2-NiO nanoflakes with high areal pseudocapacitance. *J. Mater. Chem.* **22**, 2419 (2012).
24. Xiao, J. W., Wan, L., Yang, S. H., Xiao, F. & Wang, S. A. Design hierarchical electrodes with highly conductive $NiCo_2S_4$ nanotube arrays grown on carbon fiber paper for high-performance pseudocapacitors. *Nano Lett.* **14**, 831 (2014).
25. Xu, K. B. *et al*. Hierarchical mesoporous $NiCo_2O_4$@MnO_2 core-shell nanowire arrays on nickel foam for aqueous asymmetric supercapacitors. *J. Mater. Chem. A* **2**, 4795 (2014).
26. Xia, X. H. *et al*. Synthesis of free-standing metal sulfide nanoarrays via anion exchange reaction and their electrochemical energy storage application. *Small* **10**, 766 (2014).
27. Rakhi, R. B., Chen, W., Cha, D. & Alshareef, H. N. Substrate dependent self-organization of mesoporous cobalt oxide nanowires with remarkable pseudocapacitance. *Nano Lett.* **12**, 2559 (2012).
28. Wang, H. L., Gao, Q. M. & Jiang, L. Facile approach to prepare nickel cobaltite nanowire materials for supercapacitors. *Small* **7**, 2454 (2011).
29. Xu, Y. *et al*. Facile synthesis route of porous $MnCo_2O_4$ and $CoMn_2O_4$ nanowires and their excellent electrochemical properties in supercapacitors. *J. Mater. Chem. A* **2**, 16480 (2014).
30. Lu, X. H. *et al*. Facile synthesis of large-area manganese oxide nanorod arrays as a high-performance electrochemical supercapacitor. *Energy Environ. Sci.* **4**, 2915 (2011).
31. Li, X. W., Xiong, S. L., Li, J. F., Bai, J. & Qian, Y. T. Mesoporous NiO ultrathin nanowire networks topotactically transformed from α-$Ni(OH)_2$ hierarchical microspheres and their superior electrochemical capacitance properties and excellent capability for water treatment. *J. Mater. Chem.* **22**, 14276 (2012).
32. Mai, L. Q. *et al.* Hierarchical $MnMoO_4$/$CoMoO_4$ heterostructured nanowires with enhanced supercapacitor performance. *Nat. Commun.* **2**, 381 (2011).
33. Cheng, C. & Fan, H. J. Branched nanowires: synthesis and energy applications. *Nano Today* **7**, 327 (2012).
34. Liu, C., Tang, J. Y., Chen, H. M., Liu, B. & Yang, P. D. A fully integrated nanosystem of semiconductor nanowires for direct solar water splitting. *Nano Lett.* **13**, 2989 (2013).
35. Yuan, C. Z. *et al.* Ultrathin mesoporous $NiCo_2O_4$ nanosheets supported on Ni foam as advanced electrodes for supercapacitors. *Adv. Funct. Mater.* **22**, 4592 (2012).
36. Zhang, G. Q. & Lou, X. W. General solution growth of mesoporous $NiCo_2O_4$ nanosheets on various conductive substrates as high-Performance electrodes for supercapacitors. *Adv. Mater.* **25**, 976 (2013).
37. Xia, X. H. *et al*. High-quality metal oxide core/shell nanowire arrays on conductive substrates for electrochemical energy storage. *ACS Nano* **6**, 5531 (2012).
38. Kim, J. H., Zhu, K., Yan, Y., Perkins, C. L. & Frank, A. J. *Nano Lett.* **10**, 4099 (2010).
39. Liu, X. Y. *et al*. Hierarchical $NiCo_2O_4$@$NiCo_2O_4$ core/shell nanoflake arrays as high-performance supercapacitor materials. *ACS Appl. Mater. Interfaces* **5**, 8790 (2013).

Acknowledgments

This work was financially supported by the National Natural Science Foundation of China (Grant Nos. 5034301, 21171035 and 51302035), the PhD Programs Foundation of the Ministry of Education of China (Grant Nos. 20110075110008 and 20130075120001), the Hong Kong Scholars Program, the Science and Technology Commission of Shanghai Municipality (Grant No. 13ZR1451200), the Project funded by China Postdoctoral Science Foundation, the Key Grant Project of Chinese Ministry of Education (Grant No. 313015), the National 863 Program of China (Grant No. 2013AA031903), the Shanghai University Young Teacher Training Program, and the Fundamental Research Funds for the Central Universities.

Author contributions

R.J.Z. and Z.Y.Z. contributed equally to this work. R.J.Z. and Z.Y.Z. designed and performed the experiments. R.J.Z., Z.Y.Z. and M.F.Y. prepared the samples and analyzed the data. R.J.Z., J.Q.H., C.S.L. and W.J.Z. participated in interpreting and analyzing the data. R.J.Z., Z.Y.Z. and W.J.Z. wrote the manuscript.

Additional information

Supplementary information accompanies this paper at http://www.nature.com/scientificreports

Competing financial interests: The authors declare no competing financial interests.

How to cite this article: Zou, R. *et al*. Dendritic Heterojunction Nanowire Arrays for High-Performance Supercapacitors. *Sci. Rep.* **5**, 7862; DOI:10.1038/srep07862 (2015).